

## NUMERICAL SIMULATION AND EXPERIMENTAL CALCULATION OF THE SHEAR VELOCITY OVER REGULARLY SPACED HEMISPHERES

Elena IATAN<sup>1</sup>, Florin BODE<sup>2</sup>, Ilinca NASTASE<sup>3</sup>,  
Radu Mircea DAMIAN<sup>4</sup>

*In the study of flows over rough surfaces there is a vulnerable point in the determination of the shear velocity. The authors performed a numerical study whose results are the data enabling calculation of local shear velocity using the Turbulent Kinetic Energy approach. The employed numerical method is Large Eddy Simulation. The numerical results are validated by comparison with Particle Image Velocimetry experimental results. A different method, derived from the Turbulent Kinetic Energy approach, is also used to calculate shear velocity from the experimental results.*

**Keywords:** artificial roughness, Large Eddy Simulation, shear velocity, Particle Image Velocimetry

### 1. Introduction

The efficiency of the commonly accepted design criteria of a self-cleaning sewer is questionable [1] because it specifies a minimum mean velocity for the flowing water not considering the characteristics of transported sediments or the intermittent nature of the flow. In this situation, during the exploitation time of a sewer pipe, the failure of these self-cleaning criteria will be frequently observed in the deposition of some of the transported particles. The resulted sediment deposits will generate additional roughness elements at the boundary of the pipe. This is demonstrated to increase the turbulence intensity leading to momentum extraction from the mean flow and to modify the hydraulic performances of the sewer pipe. In the design phase of a sewer system, the considered values of roughness coefficients correspond to the case of new clean pipes transporting clear water. The apparition of deposits at the boundary of a sewer pipe can be expressed also by modifications of the roughness coefficient, and for sewers design the most commonly used is the Manning roughness coefficient. That discrepancy between the exploitation and the design phase lead us to the study of roughness

<sup>1</sup> Technical University Of Civil Engineering, Bucharest, Romania, email:iatan.elena@gmail.com

<sup>2</sup> Technical University Cluj-Napoca, Romania, email: florin.bode@termo.utcluj.ro

<sup>3</sup> Technical University Of Civil Engineering, Bucharest, Romania, email: ilinca.nastase@cambi.ro

<sup>4</sup> Technical University Of Civil Engineering, Bucharest, Romania, email: damian@astralnet.ro

coefficients. Our first aim is to evaluate the roughness coefficients in the situation of a free surface flow over artificially created roughness elements at the bottom wall. Even if the characteristics of a flow over idealized roughness elements may not be completely extrapolate to practical situations, most of the reported studies dealt with laboratory roughness. One critical element of experiments concerning flows over rough surfaces is the determination of the shear velocity as shear velocity is an important parameter involved in the calculation of Manning roughness coefficient. Another important application of this parameter is related to the characterization of sediments transport and pollutants dispersion [2], the shear velocity is also frequently used for scaling turbulence parameters.

It is widely known that the wall shear stress is defined as  $\tau = \mu \cdot \partial u / \partial y|_{wall}$  (where  $\tau$  is the shear stress,  $\mu$  is the dynamic viscosity of the fluid,  $u$  is the fluid velocity and  $y$  is the height above the wall). The notion of shear velocity is a relatively artificial quantity representing the shear stress expressed in velocity units to achieve a more comfortable manipulation. Considering the relationship between the shear velocity and the shear stress,  $\tau = \rho u_*^2$  (where  $u_*$  is the shear velocity), we notice that this quadric relation requires a very precise estimation of the shear velocity to have reliable shear stress values as shear stress is a difficult measure to obtain. Shear stress measurement techniques are usually divided into direct and indirect methods. In the literature direct measurement techniques are presented in Carvalho et al. [3]. Hot wire and hot films sensors need a precise calibration and the results can be affected by sensor drift. Surface mounted force balance calculates a spatial averaging of the shear stress over the sensor surface and has poor high-frequency response. A general conclusion is that a complete distribution of the wall shear stress is still difficult to experimentally achieve. Indirect methods are also presented in the literature, based on Laser Doppler Velocimetry (LDV) [4], Particle Image Velocimetry (PIV) [5], nonintrusive methods, but depend on theoretical formulations to obtain the values of bed shear stress. Indirect methods have been adopted in different studies due to difficulties in obtaining direct bed shear stresses from the flow field.

In this section we briefly describe some of the main methods, detailed in the literature, in order to calculate the shear velocity. The log profile method (LOG) is based on the semi-logarithmic representation of the velocity distribution [6]. This popular method is strongly influenced by the position of the first point, relatively to the bottom wall, involved in the semi-logarithmic distribution. From our previous experience this method can strongly overrate the values of shear velocity and is usually involved in the study of simple flows. If turbulence measurements are available we may also calculate the local shear velocity in several ways. A first possible procedure is to extrapolate the linear portion of the Reynolds shear stress distribution (RSS) to the bed [7]. The intercept will

correspond to the value of the shear stress at the bottom wall. Another option, if turbulence quantities are available, is the so-called Turbulent Kinetic Energy approach (TKE) and is based on a linear relation between the turbulent kinetic energy and the bottom shear stress,  $\tau = Ct \cdot K$  where  $Ct$  is a proportionality constant considered to be equal to 0,19. In the literature there are also variations of the Turbulent Kinetic Energy approach that consider the distribution of the turbulent intensities in only one of the three directions (TKEw). Biron et al. [8] and Rowinsky et al. [9] observed a good agreement between RSS and TKE methods. Also they noticed important differences between LOG method and the other methods in the case of flows over roughness elements. In the present study TKE method is applied to the numerical results and TKEw method is applied to the experimental results.

A different method used for the Reynolds Stresses estimation is the Computational Fluid Dynamics method (CFD). The most accurate results for the numerical simulations are provided by the Direct Numerical Simulation (DNS) where the flow is numerically solved using Navier–Stokes equations without including a turbulence model [10], [11]. The computational cost of DNS is very high, even at very low Reynolds numbers, therefore other methods are used in research and industry for the numerical simulation of flows. Most of the numerical studies of the fluid flows over roughness elements use the Reynolds-Averaged Navier-Stokes (RANS) method with different turbulence models. A general feature of these studies is that the calculated velocity profiles find a good match with the experimental profiles; at the same time important differences are observed between the calculated and measured components of the turbulent kinetic energy, especially in the near-wall region. From our previous experience [12] we evidence that using RANS the same qualitative results are observed only for the mean flow features. We estimate that for precise information on turbulent structures, Large Eddy Simulation method (LES) could be an appropriate tool. This method solves the transport equations corresponding to the scales of motion larger than the chosen grid size, for the scales smaller than this limit subgrid-scale models are used. This paper is based on a Large Eddy Simulation study in order to estimate the shear velocity (replaceable with the shear stress) from the distribution of the turbulent kinetic energy.

After the filtering operation the resulting subgrid-scale stresses are unknown and usually they are fully modeled in LES methods. Important studies in the literature are based on LES, [13], [14] with various subgrid-scale models. In contrast to large-scale turbulence structures, for the small scales of a turbulent motion the tendency is to consider them as isotropic and with a higher universality degree. Small eddies have little contribution to momentum transport so that a LES is expected to be little sensitive to the adopted model [15]. Sophisticated subgrid-

scale models are developing but simple models, like the Smagorinsky model, are still commonly used and considered a classic choice.

## 2. Numerical method, flow geometry and boundary conditions

Large Eddy Simulation resolves the transport equations for all the turbulent motion scales larger than the established grid size. To separate large scales from small scales the main operation in the LES method is low-pass filtering. This operation is applied to the Navier–Stokes equations to eliminate small scales of the solution. The scales smaller than the grid size are solved using subgrid-scale models. This operation reduces the computational cost of the numerical simulation. The governing equations are thus transformed, and the solution is a filtered velocity field. In LES we must model  $\tau_{ij}$ , the subgrid-scale stresses, that is three-dimensional and time-dependent. Subgrid-stress models must represent the momentum fluxes transferred by most of the eddies. One of the frequently adopted solutions for the subgrid-scales is the Smagorinsky-Lilly model, presented in equations (2). Details of the filtration procedure can be found in [16]. Relations (1) show the filtered Navier-Stokes equations for an incompressible flow.

$$\begin{aligned} \frac{\partial \bar{u}_i}{\partial x_i} &= 0, \\ \frac{\partial \bar{u}_i}{\partial t} + \frac{\partial}{\partial x_j} (\bar{u}_i \bar{u}_j) &= -\frac{1}{\rho} \frac{\partial \bar{p}}{\partial x_i} - \frac{\partial \tau_{ij}}{\partial x_j} + \vartheta \frac{\partial^2 \bar{u}_i}{\partial x_j \partial x_j} \end{aligned} \quad (1)$$

$\bar{u}_i$  is the filtered velocity component in the  $x_i$  direction,  $x_i$  are tensor coordinates in space,  $t$  is time,  $\tau_{ij}$  is the subgrid – scale stress tensor,  $\vartheta$  is the water kinematic viscosity,  $\rho$  is the density and  $\bar{p}$  is the filtered pressure.

$$\begin{aligned} \tau_{ij} &= -2\mu_t \bar{S}_{ij} \\ \mu_t &= \rho L_s^2 \sqrt{2S_{ij}S_{ij}} \\ L_s &= \min(\kappa d, C_s \Delta) \end{aligned} \quad (2)$$

$\mu_t$  is the subgrid turbulent viscosity,  $C_s$  is the Smagorinsky parameter that determines the effectiveness with which kinetic energy is dissipated from the resolved velocity field during LES,  $L_s$  is the mixing length,  $\kappa$  is the Karman constant,  $d$  is the distance to the closest wall and  $\Delta$  is the local grid scale calculated with  $V^{1/3}$  and  $V$  is the volume of the computational cell,

$$\Delta = V^{1/3} \quad (3)$$

Numerical calculations were performed for a calculation field that reproduces the geometrical and experimental flow conditions. In the experimental set-up, the flow is confined by a plexiglas pipe having the geometrical dimensions presented in Fig. 1a).

The specified velocity inlet in the calculation domain is 0,25 m/s. The outlet pressure is the atmospheric pressure and the depth of the flow is around 68 mm. At the rigid bottom walls we imposed the no-slip condition and respectively the slip condition at the free surface. Also, on the inlet boundary an artificial resolved turbulence was imposed using Vortex Method for the Fluctuating Velocity Algorithm. As for the turbulence conditions specification method we choose Intensity and Hydraulic Diameter. The imposed Turbulent Intensity,  $I$ , is equal to 5,36% and was calculated using the relation  $I = 0,16 \times \text{Re}^{-1/8}$  see [17], where  $\text{Re}$  is the bulk Reynolds number. The Reynolds number, in terms of mean velocity and hydraulic radius, is around 7200. The definition of the Reynolds number is  $\text{Re} = L \times u / \vartheta$  where  $L$  is the characteristic length scale considered equal to the hydraulic radius ( $R_h = 0,0245 \text{ m}$ ),  $u$  is the mean velocity (0,25 m/s for a flow rate equal to 1,20 l/s) and  $\vartheta$  is the water kinematic viscosity  $0,85 \times 10^{-6} (\text{m}^2/\text{s})$ .

Artificial roughness elements are represented by 4,5 mm diameter hemispheres placed at the bottom wall, the ratio  $p/k$  is equal to 4 in the stream-wise direction, see Fig. 1b).

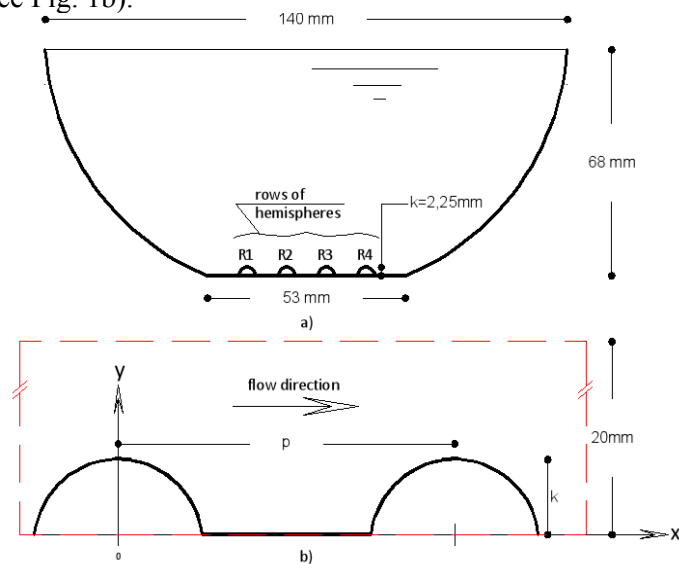


Fig. 1. Model configuration. Fig. 1a) pipe section perpendicular to the flow direction, R1, R2, R3 and R4 are the equally spaced rows of hemispheres. Fig. 1b) configuration of the two successive hemispheres aligned in the flow direction. The measurements are realized over the entire depth of the flow (68mm) and with a zoom at the bottom wall containing 20mm from the depth of the flow.

The accepted classification of roughness surfaces designates either “k-” or “d-” type behavior (the terminology of Perry et al., 1969), in this context d stands for the pipe diameter and k stands for the height of the roughness. In case of a k-type behavior the roughness function (the displacement of the velocity profile) depends on the height of the roughness element. If the roughness function can be expressed through a relationship that involves the pipe diameter we are dealing with a d-type surface. Attempts are made in order to identify a sharp delimitation between k-type and d-type but this discussion is beyond the purpose of the present paper. Usually, for  $p/k$  values greater or equal to 4 we are dealing with a k-type surface.

For the geometrical discretization we used polyhedral cells because are producing equivalent accuracy results compared to other mesh types and they offer some other benefits, like faster convergence in a fewer number of iterations, robust convergence to lower residual values than other mesh types and therefore this will lead to faster solution runtimes.

A grid independence test was carried out, for which we have generated three different polyhedral meshes: 0,3, 0,64 and 1,45 million of polyhedrons (see Fig. 2). The number of nodes corresponding to the analyzed meshes was: 1,79, 3,31 and 7,71 million of nodes. The results obtained with the 0,64 and 1,45 million elements, in terms of velocity profiles, were similar with the results obtained by PIV technique, therefore for the following studies we chose the 0,64 million of polyhedron elements. Cell Reynolds number vary from 0,038 to 403 in the interest domain.

### **3. Velocity profiles and streamlines, comparison with experimental measurements**

As stated before, the geometrical model that we used in numerical simulation is designed to have identical characteristics with the experimental model and specific details for both cases are presented in Fig. 1. The technology that we use to apply the roughness elements at the bottom wall, in the experimental model, make the roughness heights of the hemispheres to vary between 1,9 and 2,25 mm and the ratio  $p/k$  may locally vary between 4,8 and respectively 4. Bulk Reynolds number in the model is equal with the Reynolds number in the experiment, namely  $Re=7200$ . For the validation of the LES model we compare streamwise velocity profiles on the top of the roughness element (profile 1 – see Fig. 3. a) and in the cavity created between two consecutive roughness elements (profile 2 – see Fig. 3. b) with corresponding profiles of experimental data. PIV data are obtained from zoom view measurements at the bottom wall along profiles 1 and 2. All of the PIV data are taken from a longitudinal plane in the middle of the row R3 (see Fig. 1.).

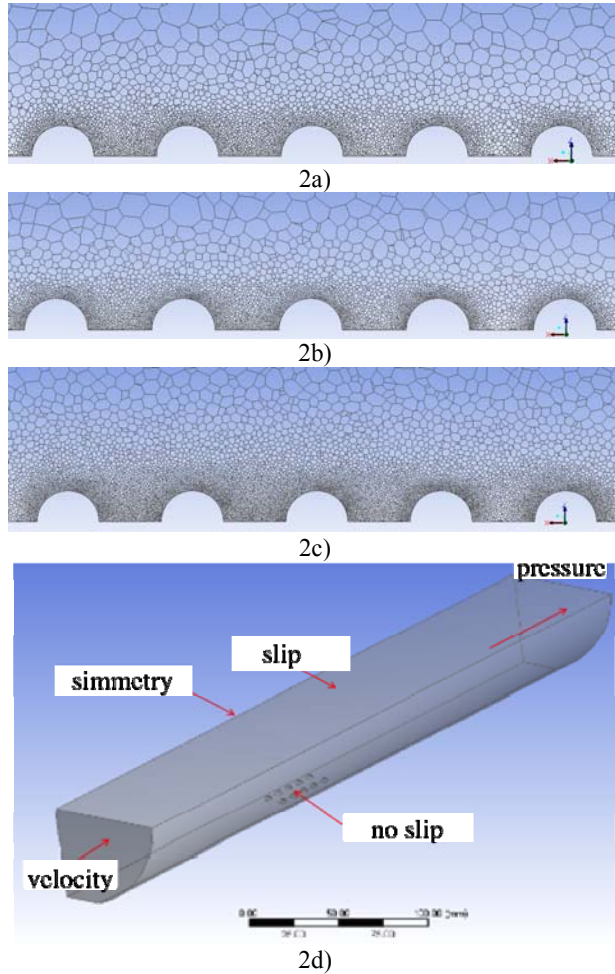


Fig. 2. 2a) Discretization domain with 0,3 million polyhedron elements, 2b) 0,64 million respectively 2c) 1,45 million polyhedron elements, 2d) Detailed representation of the discretization domain in the flow direction, for LES at  $p/k=4$ , 0,64 million elements, only the third and the fourth rows of hemispheres are represented.

For numerical validation we first compared the numerical results in terms of velocity profiles with the PIV experimental results (see Fig. 3). For profile 2 we observe a negative value of the velocity corresponding to the reversed flow and after reaching a minimal value the growth is almost linear. There is a good agreement between the experimental values and numerical calculation. Similar variations of the velocity profiles are presented in the literature [12]. Comparative streamlines around two consecutives hemispheres of results obtained also by the two situations (PIV measurements and LES simulations) are displayed in Fig 4. In

the PIV measurements, starting with the height of a roughness element, over the top of the hemispheres, the streamlines are nearly parallel.

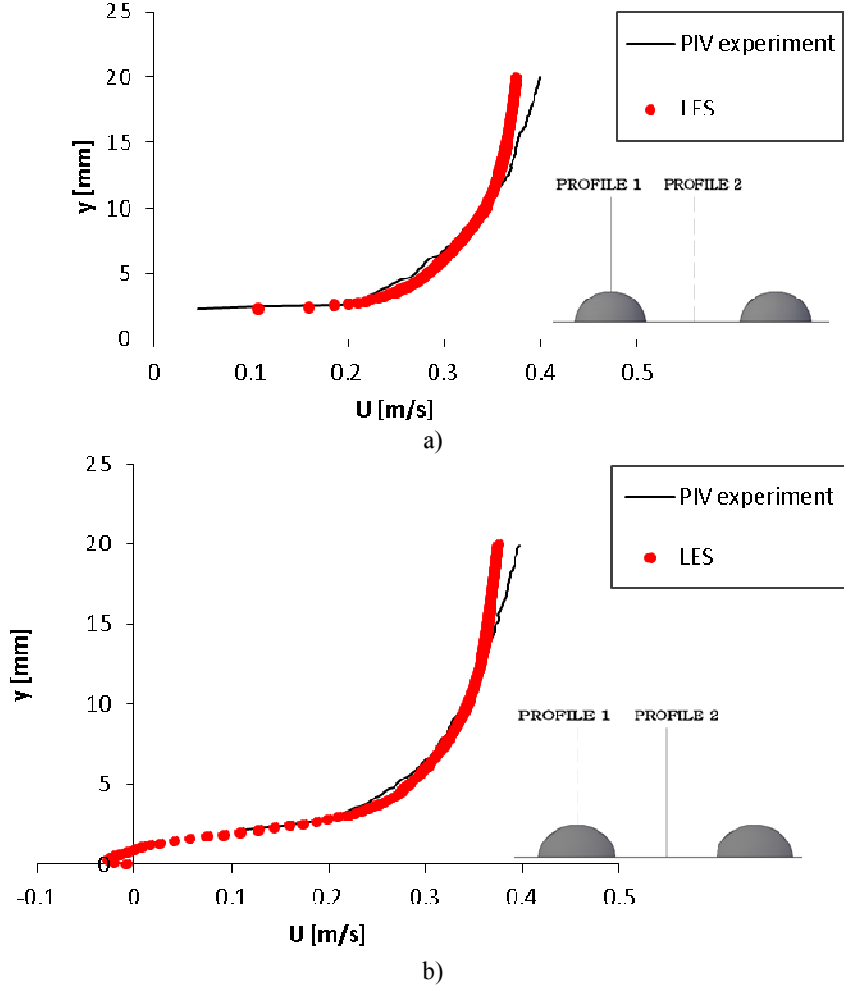


Fig. 3. Mean velocity profiles from PIV measurements and LES calculations, figure 3a) for the streamwise velocities over the depth of profile 1, respectively 3b) over the depth of profile 2.  $Re=7200$ . PIV measurements are performed with a zoom at the bottom wall level; only 20mm of the entire depth are visible in this procedure.

We notice that in the LES calculations the velocity contours are becoming parallel starting with half of the height of a roughness element. During the experiments this stronger interaction between the flow inside the cavity and the flow outside of the hemispheres is legitimate by the values of  $p/k=4,8$  instead of 4 as explained above. A vortex is observed inside the cavity, we notice that the vortex position, closer to the second hemisphere along to the flow direction, corresponds in the

literature [5]. The experimentally observed maximum values of the turbulence intensities correspond to a k-type surface with the ratio  $p/k$  equal 4 [5].

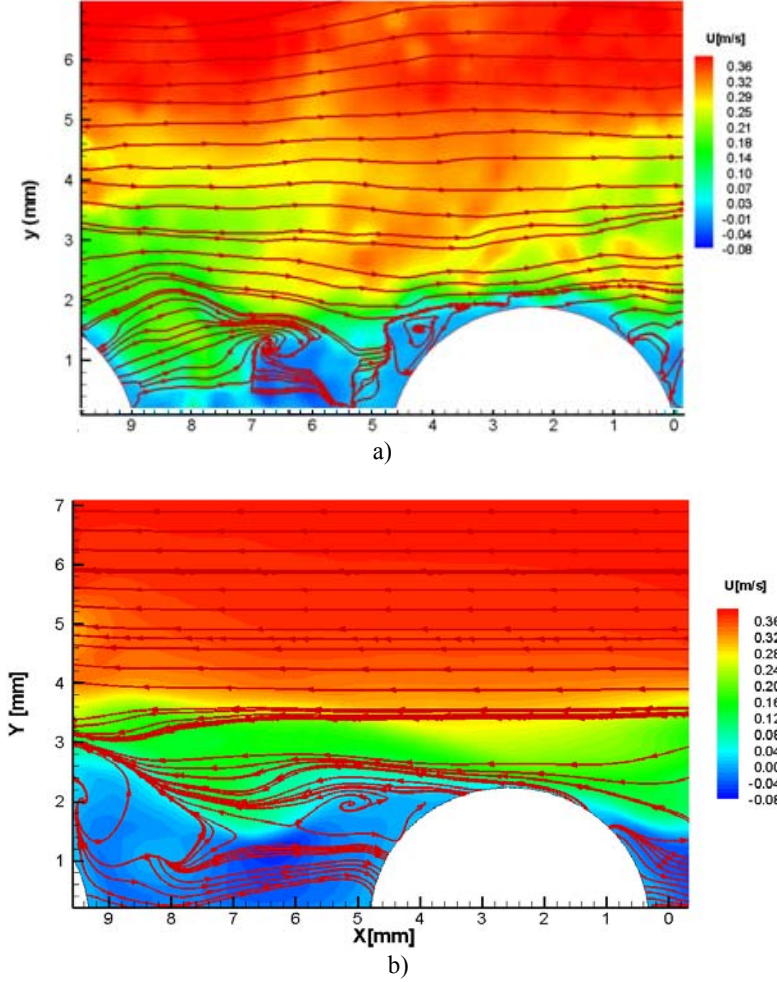


Fig. 4. Comparison between streamlines superposed over velocity fields Fig. 4a) for PIV measurements and Fig. 4b) for LES simulation data.  $Re=7200$ . In order to compare the experimental and numerical results around the hemispheres area we have choose a representation depth of 7mm, in both cases.

The streamlines close to the hemispheres are not parallel, indicating an important interaction between the flow inside the cavity and the outer flow; this feature is characteristic to the k-type roughness. Images at only 7mm from the depth of the flow are presented in Fig. 4 because the streamlines have already become parallel at that depth of the water.

#### 4. Shear velocity calculation

Recent studies performed by Pope et al. [19] suggest that the Turbulent Kinetic Energy approach is probably one of the most unfailing methods to estimate bed shear stress (replaceable with the shear velocity). This approach is based on a simple linear relation between the turbulent kinetic energy and shear stress, relation that is present in turbulence models, like  $k-\omega$  SST see Wilcox [20]. Equation (4) relates the shear stress to the turbulent kinetic energy and it was used to calculate the distributions presented in Fig. 5.

$$\tau_t = C_1 \left[ 0,5 \left( \bar{u'}^2 + \bar{v'}^2 + \bar{w'}^2 \right) \right] \quad (4)$$

where  $\tau_t$  is the bed shear stress,  $C_1$  is the proportionality constant with suggested values of 0,19 or 0,21 [7],  $u'$ ,  $v'$  and  $w'$  are the fluctuating components of velocity. Summing velocity variances forms the turbulent kinetic energy. In this study  $C_1$  was considered equal to 0,19, see [21].

Relation (4) is based on Bradshaw assumption (1967) which states that the principal turbulent shear stress is proportional to turbulent kinetic energy; this assumption is often associated with local equilibrium. Relation (4) is not valid in the viscous sublayer where velocity fluctuations vanish. In this study we are dealing with a hydraulic roughness regime, the superior limit of the viscous sublayer is below the 2,25mm that is the corresponding height of the hemisphere. A maximum value of the shear stress is observed at about 6% of the depth of the flow which is above the roughness height (see Fig. 5). A similar distribution of the turbulent kinetic energy in literature presents a maximum at around 10% of the depth of the flow, [5]. We considered that we might further use the LES simulation to calculate the shear stress (replaceable with the shear velocity) from the distribution of the turbulent kinetic energy. The numerical results are presented in Fig. 5.

Using maximum values of the shear stress 0,51 (N/m<sup>2</sup>) along the profile 1 and respectively 0,68 (N/m<sup>2</sup>) for profile 2 (see the dashed lines in Fig. 5) we calculate the correspondent shear velocities 0,023 m/s and 0,026 m/s.

Further, we employ our experimental results to calculate the shear velocity in order to compare with the numerical calculated values. Experimental data are handled with a method proposed by Nezu & Nakagawa [22] which is a profile matching technique. For the free surface flows they observed a “universality” feature of the profiles of root mean square distribution of velocity fluctuations. One of these empirical observed distributions are given in equation (5) from measurements in the streamwise direction.

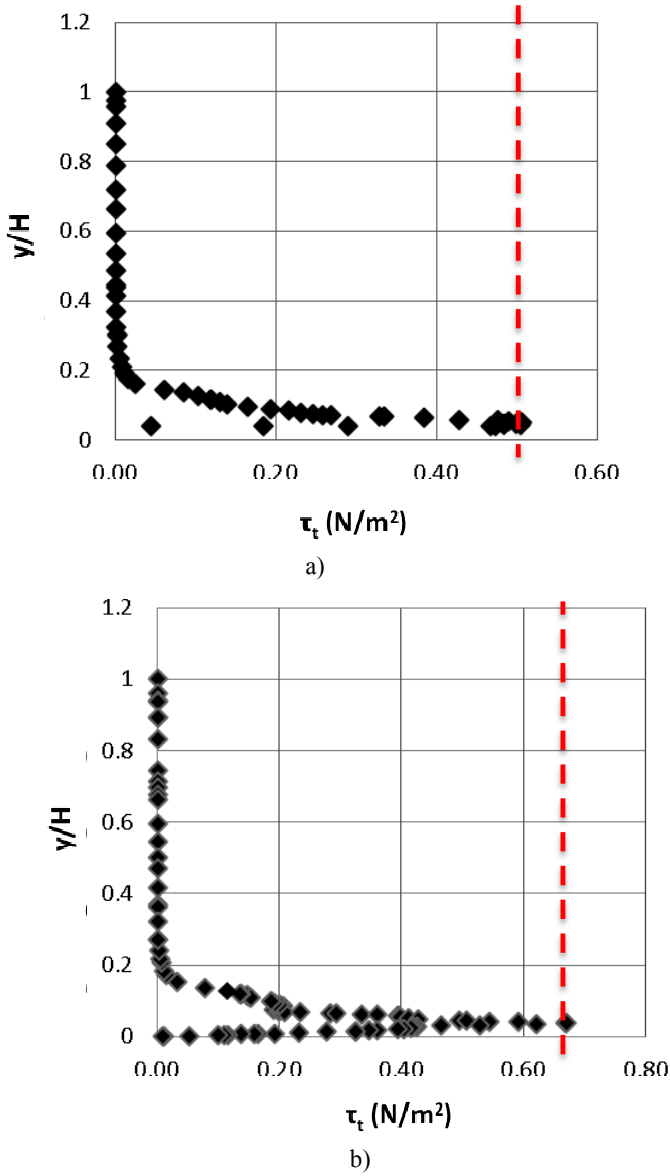


Fig. 5). Distribution of shear stress over the depth of the flow for profile 1 in figure 5a) respectively for profile 2 in figure 5b). These distributions are obtained using LES for  $Re=7200$ .

The procedure consists in iterative proposed values for the shear velocity until the experimental distribution matches the theoretical distribution in equation (5). The fitting coefficient between the two sets of data (theoretical and experimental distributions) has values greater than 0,95.

$$\frac{u_{rms}}{u_*} = 2,3 \exp\left(\frac{-y}{h}\right) \quad (5)$$

where  $u_{rms}$  is the root mean square of velocity fluctuations obtained from PIV experiment,  $u_*$  is the shear velocity,  $h$  is the depth of the flow equal to 68mm and  $y$  is a certain level over the depth of the flow. Figure 6 shows the final match of the two distributions (the theoretical distribution and the experimental one).

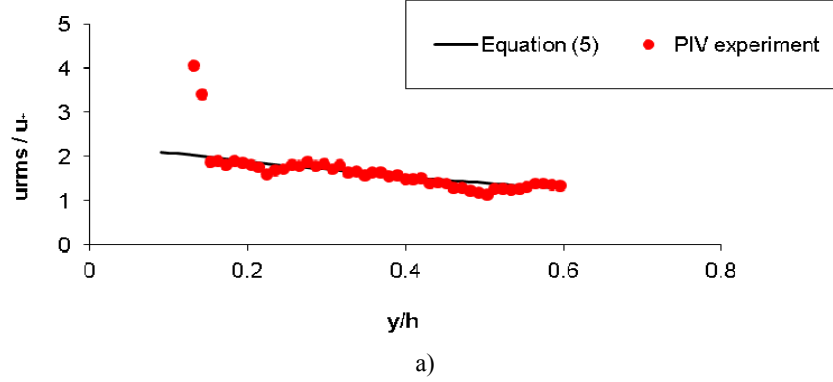
The values of the shear velocities calculated in this chapter are centralized in Table 1.

Table 1

**Shear velocity calculations, for a bulk Re=7200**

| Local position | $u_*$ (m/s)              |                           |
|----------------|--------------------------|---------------------------|
|                | TKE method from LES data | TKEw method from PIV data |
| Profile 1      | 0,023                    | 0,026                     |
| Profile 2      | 0,026                    | 0,024                     |

In an open channel study over a layer of spheres Manes et al. [23] calculated the shear velocity, using the extrapolation of the spatially averaged Reynolds stress to the bed, they obtained a value of 0,023m/s. The spheres with a 12mm diameter were made of glass and packed in a cubic pattern, tangent to each other. Bulk Reynolds number was equal to 7200. Velocity results in the study mentioned above are obtained also using the PIV technique. Carvalho et al. [3] performed a study in an open channel flow over a wall covered with 4mm glass spheres in a triangular arrangement; the spheres were also tangent to each other. The calculated shear velocity has values between 0,0442m/s and 0,0679m/s. The highest value is calculated from the LOG method and the smallest is obtained from the extrapolation of the Reynolds stress. The bulk Reynolds number in [3] was equal to 11000 and the LDV technique was used for velocity measurements. Comparing the values of the shear velocity presented in Table 1 with similar studies in the literature [3] and [23] we observe that, at least as an order of magnitude, the results presented in this paper can be considered as reliable.



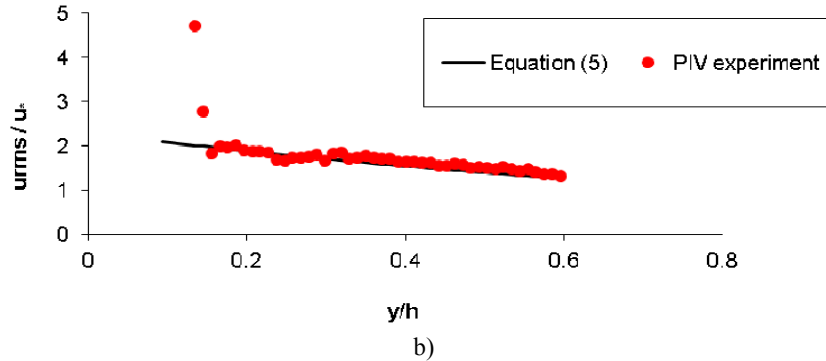


Fig. 6. Calculation of shear velocity from experimental results, Fig. 6a) for the position of profile 1, and Fig. 6b) for the position of profile 2.  $Re=7200$ .

## 5. Conclusions

We performed a numerical simulation of a flow over hemispherical roughness elements using Large Eddy Simulation. The numerical model that was carried out in this paper is designed to be identical with an experimental previously investigated model. However, small geometrical differences exist and are reflected in the experimental results by a more important interaction between the flow inside the cavity and the flow layer above of the roughness elements. The present simulation agrees well with the laboratory experiments. The aim of the numerical simulation was to obtain the local shear stress from the calculated distribution of the turbulent kinetic energy, which could not be obtained by the experimental study because in the PIV measurements we investigate the flow velocity in the streamwise and spanwise directions only. The advantage offered by the numerical simulation is a three-dimensional representation of the flow that enables us to calculate the turbulent kinetic energy. A supplementary validation of the calculated shear velocity using the numerical simulation is obtained by comparison with similar results that involve a matching technique applied to Particle Image Velocimetry experiments.

## REFERENCE

- [1]. *Charles H.J. Bong*, A Review on the Self-Cleansing Design Criteria for Sewer System, UNIMAS e-Journal of Civil Engineering, October 2014.
- [2]. *Marcus Schulz, Jan Priegnitz, Jörg Klasmeier, Stefan Heller, Stefan Meinecke, Michael Feibicke*, Effect of bed surface roughness on longitudinal dispersion in artificial open channels, *Hydrological Processes*, Volume 26, Issue 2, pages 272–280, 15 January 2012, Wiley Online Library.
- [3]. *Elsa Carvalho, Rodrigo Maia, M. F. Proença*, Shear Stress Measurements over Smooth and Rough Channel Beds, *River Flow 2010*, Dittrich, Koll, Aberle & Geisenheimer (eds) - © 2010 Bundesanstalt für Wasserbau ISBN 978-3-939230-00-7.

[4]. *Ryoichi Kurose, Satoru Komori, Turbulence structure over a particle roughness*, International Journal of Multiphase Flow, Volume 27, Issue 4, April 2001, Pages 673–683, Elsevier.

[5]. *Martin Agelinchaab, Mark F. Tachie, Open channel turbulent flow over hemispherical ribs*, 2006, International Journal of Heat and Fluid Flow 27 1010-1027, Elsevier.

[6]. *Ebenezer Ekow Essel, Mark Francis Tachie, Roughness Effects on Turbulent Flow Downstream of a Backward Facing Step, Flow, Turbulence and Combustion*, January 2015, Volume 94, Issue 1, pp 125-153, Springer.

[7]. *Herrmann Schlichting*, Boundary-Layer Theory, 2000, ISBN 978-3-540-66270-9, Springer.

[8]. *Pascale M. Biron, Stuart N. Lane, André G. Roy, Kate F. Bradbrook, Keith S. Richards*, Sensitivity of bed shear stress estimated from vertical velocity profiles: the problem of sampling resolution, Earth Surface Processes and Landforms, Volume 23, Issue 2, 133–139, February 1998.

[9]. *Pawel M. Rowinski, Jochen Aberle, Agata Mazurczyk*, Shear velocity estimation in hydraulic research, Acta Geophysica Polonica, Vol. 53, No. 4, pp. 567-583, 2005.

[10]. *Paolo Orlandi, Stefano Leonardi*, DNS of turbulent channel flows with two- and three-dimensional roughness, Journal of Turbulence Volume 7, No. 53, 2006, Taylor & Francis.

[11]. *Paolo Orlandi*, DNS of transitional rough channels, Journal of Turbulence Vol. 12, No. 29, 2011, 1–20, Taylor & Francis.

[12]. *Elena Șerban*, Contribuții la studiul efectelor poluării accidentale în rețele urbane de canalizare, Teză de doctorat, Universitatea Tehnică de Construcții București (Technical University of Civil Engineering Bucharest), octombrie 2012.

[13]. *Chris D. Dritsiris*, Large eddy simulation of turbulent channel flow with transverse roughness elements on one wall, International Journal of Heat and Fluid Flow, Volume 50, December 2014, Pages 225–239.

[14]. *Sowjanya Vijiapurapu, Jie Cui*, Performance of turbulence models for flows through rough pipes, Applied Mathematical Modelling, 34, 1458–1466, Elsevier, 2010.

[15]. *Michele Ciofalo*, Large-Eddy Simulation: A Critical Survey of Models and Applications. Advances in Heat Transfer Volume 25, 321-419, 1994.

[16]. *Stefano Leonardi, Fabrizio Tessicini, Paolo Orlandi, Robert Antonia*, Direct numerical and large-eddy simulations of turbulent flows over rough surfaces, AIAA Journal, 11/2006, Volume 44, Issue 11, 2482 – 2487, Elsevier.

[17]. *Julian E. Jaramillo, Carlos-David Perez-Segarra, Ivette Rodriguez, Assensi Oliva, Numerical*, Study of plane and round impinging jets using RANS models. Numer. Heat Transfer Part B, 2008. 54: p. 213-237.

[18]. *Stefano Leonardi, Paolo Orlandi, Robert A. Antonia*, Properties of d- and k-type roughness in a turbulent channel flow, Physics of Fluids 19, 125101, 2007.

[19]. *Christopher N. Pope, John Widdows, M. D. Brinsley*, Estimation of bed shear stress using the turbulent kinetic energy approach—A comparison of annular flume and field data, Continental Shelf Research, Volume 26, Issue 8, June 2006, Pages 959–970.

[20]. *David C. Wilcox*, Turbulence Modelling for CFD, Published: DCW Industries, Inc. (November 2006).

[21]. *Pascale M. Biron, Colleen Robson, Michel F. Lapointe, Susan J. Gaskin*, Comparing different methods of bed shear stress estimates in simple and complex flow fields. Earth Surf. Process. Landforms 29, 1403–1415, 2004.

[22]. *Iehisa Nezu, Hiroji Nakagawa*, Turbulence in open channel flows. IAHR Monograph, Balkema, Rotterdam, The Netherlands, 1993.

[23]. *Costantino Manes, Dubravka Pokrajac, Ian McEwan, Vladimir Nikora*, Turbulence structure of open channel flows over permeable and impermeable beds: A comparative study. Phisics of Fluids 21, 125109 - 2009.